Editors' Suggestion | Featured in Physics

Field Test of Twin-Field Quantum Key Distribution through Sending-or-Not-Sending over 428 km

Hui Liu,[1,2] Cong Jiang,[3] Hao-Tao Zhu,[1,2] Mi Zou,[1,2] Zong-Wen Yu,[4,5] Xiao-Long Hu,[4] Hai Xu,[4] Shizhao Ma,[3] Zhiyong Han,[3] Jiu-Peng Chen,[1,2] Yunqi Dai,[6] Shi-Biao Tang,[6] Weijun Zhang,[7] Hao Li,[7] Lixing You,[7] Zhen Wang,[7] Yong Hua,[8] Hongkun Hu,[8] Hongbo Zhang,[8] Fei Zhou,[3] Qiang Zhang,[1,2,3] Xiang-Bin Wang,[2,3,4,*] Teng-Yun Chen,[1,2,†] and Jian-Wei Pan[1,2,‡]

[1]*Hefei National Laboratory for Physical Sciences at Microscale and Department of Modern Physics, University of Science and Technology ofChina, Hefei, Anhui 230026, People's Republic of China*

[2]*CAS Center for Excellence in Quantum Information and Quantum Physics, University of Science and Technology of China, Hefei, Anhui 230026, People's Republic of China*

[3]*Jinan Institute of Quantum Technology, Jinan, Shandong 250101, People's Republic of China*

[4]*State Key Laboratory of Low Dimensional Quantum Physics, Department of Physics, Tsinghua University, Beijing 100084, People's Republic of China*

[5]*Data Communication Science and Technology Research Institute, Beijing 100191, People's Republic of China*

[6]*QuantumCTek Corporation Limited, Hefei, Anhui 230088, People's Republic of China*

[7]*State Key Laboratory of Functional Materials for Informatics, Shanghai Institute of Microsystem and Information Technology, Chinese Academy of Sciences, Shanghai 200050, People's Republic of China*

[8]*Chongqing Optoelectronics Research Institute, Chongqing 400060, People's Republic of China*

(Received 12 January 2021; accepted 10 May 2021; published 22 June 2021)

Quantum key distribution endows people with information-theoretical security in communications. Twin-field quantum key distribution (TF-QKD) has attracted considerable attention because of its outstanding key rates over long distances. Recently, several demonstrations of TF-QKD have been realized. Nevertheless, those experiments are implemented in the laboratory, and therefore a critical question remains about whether the TF-QKD is feasible in real-world circumstances. Here, by adopting the sending-or-not-sending twin-field QKD (SNS-TF-QKD) with the method of actively odd parity pairing (AOPP), we demonstrate a field-test QKD over 428 km of deployed commercial fiber and two users are physically separated by about 300 km in a straight line. To this end, we explicitly measure the relevant properties of the deployed fiber and develop a carefully designed system with high stability. The secure key rate we achieved breaks the absolute key rate limit of repeaterless QKD. The result provides a new distance record for the field test of both TF-QKD and all types of fiber-based QKD systems. Our work bridges the gap of QKD between laboratory demonstrations and practical applications and paves the way for an intercity QKD network with measurement-device-independent security.

DOI: 10.1103/PhysRevLett.126.250502

Introduction.—Since Bennet and Brassard proposed the BB84 protocol [1], quantum key distribution (QKD) has been studied extensively [2–7] towards its final goal of application in the real world. Given the fact that quantum signals cannot be amplified, the secure distance is severely limited by the channel loss. For example, considering the possible photon-number-splitting attack, the key rate of a BB84 protocol with the imperfect single-photon source is proportional to η^2, given the channel transmittance η. So far, many efforts have been made towards the more loss-tolerant QKD in practice. There are two mile-stone signs of progress towards this goal. First, the decoy-state method [8–10] can improve the key rate of coherent-state based QKD from quadratic scaling η^2 to linear scaling η, as a perfect single-photon source behaves. Importantly, the method can be applied to the measurement-device-independent QKD (MDI-QKD) successfully [11–14]. Second, the secure key rate can be further improved by twin-field QKD (TF-QKD) [15]. Similar to the MDI-QKD protocol, TF-QKD is assisted by an untrusted relay, Charlie, between Alice and Bob. However, instead of performing a two-photon Bell state measurement, TF-QKD is supposed to perform single-photon interference in Charlie, which allows it to provide a key rate in the square-root scale of the channel transmittance $O(\sqrt{\eta})$. In principle, as a relay-assisted protocol, TF-QKD can break the relayless bound which is known as the Pirandola-Laurenza-Ottaviani-Bianchi (PLOB) bound [16] and fundamentally indicates that the key rate scales linearly with η in the absence of the relay.

The real-world QKD aims to physically separate users on Earth. However, although tremendous efforts were made

into fiber-based QKD field test [17–25], the maximum fiber distance and the maximal physical separation achieved between two users is around 90 km [24] to date, and challenges for longer distances remain.

It is worth noting that experimental TF-QKD [26–31] has advanced significantly up to a distance of more than 500 km [30,31]. However, all the experiments are implemented in the laboratory with either the simulated channel loss or the optical fiber spool, leaving a vast gap between laboratory demonstrations and practical applications. Field trial of TF-QKD remains experimentally challenging.

In this work, for the first time, we present a field test of TF-QKD on the deployed commercial fiber (428 km length with 79.1 dB channel loss, buried underground, ultra-low-loss fiber, G654.E). Furthermore, it is the most extended fiber-based QKD field test without relying on trusted relays. Two users, Alice and Bob, realize the longest physical separation distance (about 300 km) in the terrestrial QKD so far, to the best of our knowledge. The secure key rate of our work breaks the absolute key rate limit of trusted-relayless QKD. The result lays the foundation for an intercity-scale QKD network in the absence of the quantum repeater.

We adopt the sending-or-not-sending (SNS) protocol [32] of TF-QKD with finite-key effects [33]. Besides, we apply the efficient error rejection method, known as actively odd parity pairing (AOPP) [34] with the finite-key effects studied in Ref. [33]. Given such an asymmetric channel, we adopt the asymmetric protocol [35] to improve the secure key rate further.

Protocol.—Consider the SNS-TF-QKD protocol proposed in Ref. [32]. Here, we implement an asymmetric three-intensity method for decoy-state analysis. To improve the key rate, we take the bit error rejection by AOPP [34] in the post data processing stage. In this way, the sending probability in signal windows can be far improved and hence the number of effective events is raised greatly. As a result, the final key rate is improved a lot especially in the case of small data size with finite key effects being considered. We use the zigzag approach to take the finite-key effects in calculating the final key rate [33].

In the protocol, Alice (Bob) randomly chooses the decoy window and signal window with probabilities $1-p_{A2}(1-p_{B2})$ and $p_{A2}(p_{B2})$, respectively. In the decoy window, both Alice and Bob prepare and send decoy pulses. In our three-intensity protocol, there are two types of decoy states in decoy windows for each party of Alice and Bob, one vacuum and one nonvacuum coherent states, of intensity μ_{A1} for Alice and μ_{B1} for Bob. Private random phase shifts of θ_A and θ_B are applied to each pulse. And in the signal window, Alice (Bob) decides to send out a phase-randomized weak coherent state pulse with intensity μ_{A2} (μ_{B2}) or a vacuum pulse with probabilities ϵ_A (ϵ_B) and $1-\epsilon_A$ ($1-\epsilon_B$), respectively. A Z window event is defined as an event that both Alice and Bob choose the signal windows. A Z window event is regarded as being effective if Charlie announces that only one detector clicked. An X window event is defined as an event that both Alice's weak coherent source pulse is μ_{A1} and the intensity of Bob's weak coherent source pulse is μ_{B1} and their phases satisfy an extra phase-slice condition to reduce the observed error rate [35]. As shown in Ref. [35], we set the condition of

$$\frac{\mu_{A_1}}{\mu_{B1}}=\frac{\epsilon_A(1-\epsilon_B)\mu_{A2}e^{-\mu_{A2}}}{\epsilon_B(1-\epsilon_A)\mu_{B2}e^{-\mu_{B2}}} \tag{1}$$

for the security of our asymmetric protocol.

An error in the X window is defined as an effective event in the X window when Charlie announces a click of right (left) while the phase difference between the pulse pair from Alice and Bob would provably cause a left (right) clicking at Charlie's measurement setup. At a signal window, Alice (Bob) puts down a bit value 1(0) when she (he) decides sending, Alice (Bob) puts down a bit value 0(1) when she (he) decides not sending. The values of e_1^{ph} and n_1, the phase-flip error rate and the number of effective single-photon events in the Z basis, can be calculated by the conventional decoy-state method [32,36]. Then we can calculate the secure key rate by the zigzag approach proposed in Ref. [33]. Calculation details are shown in Ref. [37].

Experiment.—In our field test, Alice and Bob are located in Jinan and Qingdao, respectively. The central relay Charlie is placed in Linyi, as shown in Fig. 1(a). The distance between Charlie and Alice (Bob) is 223 km with 40.5 dB channel loss (205 km with 38.6 dB channel loss).

The experimental setup is comprised of the synchronization system and the encoding and measurement system, as shown in Fig. 1(b). Alice and Bob are connected by two parallel field-deployed commercial fibers (in the same optical cable) with 428 km length each, named "synchronization channel" and "quantum channel," respectively, in the following.

The synchronization system includes two functions: (1) the clock synchronization, of which the details are shown in Ref. [37]; (2) the wavelength synchronization. The first issue that makes implementation difficult is avoiding the rapid relative phase drift caused by Alice's and Bob's lasers' wavelength difference. We realize the wavelength synchronization with the assistance of the laser injection technique [41]. A laser with 3 kHz linewidth is placed in Charlie as the master laser. The continuous-wave (cw) bright beam is produced and injected into Alice's and Bob's slave laser. To guarantee a 0 dBm cw bright beam injected into the slave laser, we add four erbium-doped fiber amplifiers (EDFAs), two of which are placed in Yiyuan and Zhucheng, respectively (as shown in Fig. 1). And the other two are added in Alice's and Bob's apparatus. A 10 GHz fiber Bragg grating (FBG) is inserted into Alice's (Bob's) apparatus to filter the amplified spontaneous emission (ASE) noise of the EDFAs.

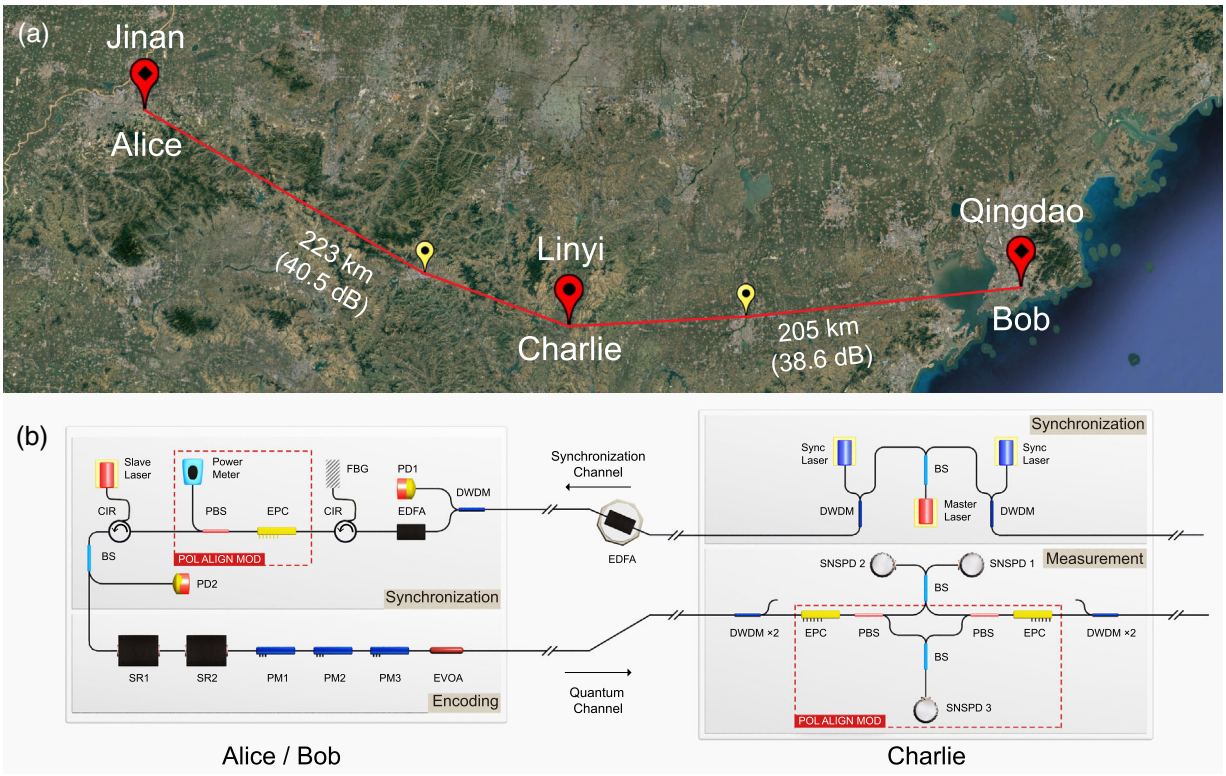

FIG. 1. (a) Bird's-eye view of our field test. Alice is located at the Jinan Institute of Quantum Technology (JIQT) in Jinan (36°41'0.60" N, 117°8'10.93" E), while Bob is located at an internet data center (IDC) room in Qingdao (36°7'24.29" N, 120°27'11.88" E). The third-party measurement is done by Charlie in a room in Linyi (36°1'39.84" N, 118°44'50.58" E), which is 223 km from Alice and 205 km from Bob. Two yellow marks show the locations of two machine rooms at Yiyuan (36° 11'12.60" N, 118° 12'24.16" E) and Zhucheng (36°2'59.31" N, 119°24'43.58" E), respectively. An erbium-doped fiber amplifier (EDFA) is placed in each machine room to amplify the light for the clock and wavelength synchronization. Map data from Google, Landsat/Copernicus. (b) Illustration of the experimental setup. A continuous-wave (cw) bright beam from a 1550.12 nm master laser is multiplexed with the pulses from two 1570 nm auxiliary synchronization lasers (Sync Lasers) in Charlie and is transmitted along the synchronization channel. The slave laser of Alice and Bob is seeded by the cw bright beam and generates pulses with a width of 320 ps and a repetition rate of 312.5 MHz. The optical launch power of the slave laser is monitored in real time by a watchdog photoelectric detector PD2 of Alice (Bob). Then these pulses are sent to two sagnac rings SR1-2, which are randomly prepared in one of the four intensities strong μ_r, high μ_{A2} (μ_{B2}), moderate μ_{A1} (μ_{B1}), and vacuum state. Three phase modulators PM1-3 are utilized for active phase randomization. The pulses are transmitted along the quantum channel and interfere in Charlie. The schematic of the polarization auto-alignment module is shown inside the red dashed rectangle. EVOA: electrical variable optical attenuator, FBG: fiber Bragg grating, CIR: circulator, EDFA: erbium-doped fiber amplifier, EPC: electric polarization controller, DWDM: dense wavelength division multiplexer, PBS: polarizing beam splitter.

The pulses produced from the slave laser pass through two sagnac rings (SRs) and three phase modulators (PMs) for encoding and phase randomization in the encoding and measurement system. The pulses are attenuated to the desired levels by an electrical variable optical attenuator (EVOA) before being transmitted to Charlie through the quantum channel. In Charlie, a 50:50 BS performs a single photon interference of the incoming pulses after noise filtering. The measurement results are detected by two superconducting nanowire single photon detectors (SNSPDs) with efficiencies of 73% and 76%, respectively. Charlie's overall detection efficiency is 28%, taking into account 2.4 dB insertion loss, 70% overlapping between signal pulse and detection window, and 94% polarization alignment efficiency. The first two terms can be measured directly. The other two are the statistical results, of which the probability distributions are shown in Figs. 3(c) and 3(d) and the details are shown in Ref. [37]. The dark count of each SNSPD is about 6 cps, corresponding to a dark count rate of 2.0×10^{-9}/pulse.

Another challenge we have encountered is the significant changes to the relative phase drift stemming from the long fiber channel. A comparison of the relative phase drift in different fiber distances in previous works and our work is shown in Fig. 1 of Ref. [37]. We stress that in our work, the signal pulses produced by the slave laser inherit the global phase of the cw bright beam, which is influenced by the 428 km synchronization channel. Then the signal pulses transmit along the 428 km quantum channel before interference. So the relative phase drift is influenced by the total 856 km fiber link, which is 7.80 rad/ms in our work. Note that in our field test, the total optical fiber

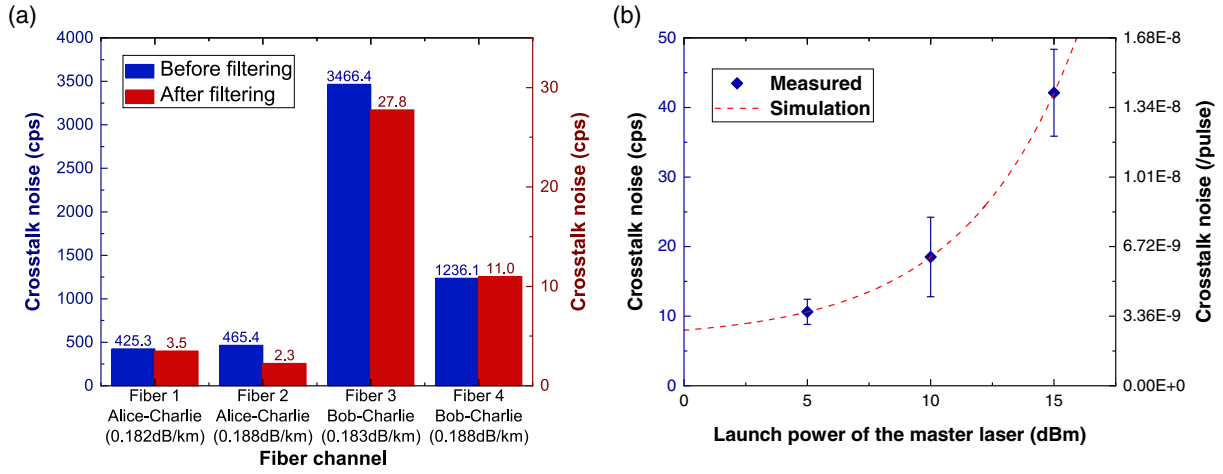

FIG. 2. Characterization of the crosstalk noise. All measurements are performed under the same overall detection efficiency (28%). (a) The crosstalk noise caused by the classical services running in some fibers in the optical cable. Without the master laser in the synchronization channel, we test two available fiber channels, fiber 1 and fiber 2 (fiber 3 and fiber 4), from Alice (Bob) to Charlie. The blue and red columns are the measurement results before and after filtering with two 100 GHz DWDMs, respectively. Note that we only need one fiber channel as the quantum channel to transmits the signal pulses from Alice (Bob) to Charlie. Taken the loss and the crosstalk noise of the fiber channel into account, we use fiber 1 (fiber 4) as the quantum channel from Alice (Bob) to Charlie. (b) The crosstalk noise caused by the cw bright beam in the synchronization channel with different optical launch power. Each experiment lasts 5 min. The experimental results are the average and variance (1 standard deviation) calculated by 144 experiments.

influencing the relative phase is longer than all the previous lab works. However, the relative phase drift is significantly lower than the 800 km result in ref [30]. It is near to most results measured in the laboratory over a shorter fiber channel. It makes the relative phase calculation in our field test much less demanding than the lab experiment in Ref. [30] over 402 km.

We verified that we could indeed estimate and compensate for the relative phase drift caused by the long fiber channel. In our work, Alice and Bob sacrifice a part of the signal pulses as bright reference pulses periodically for relative phase calculation and apply a postselection method when the signal pulse detection occurs. (for details see Refs. [30,37]). However, the scattering of the bright reference pulses will lead to nonignorable noises in the signal pulses [31]. After being filtered by four 100 GHz dense wavelength division multiplexers (DWDMs) in Charlie, the remaining noise is about 1.4×10^{-8}/pulse.

Besides, we face the crosstalk noise in the field test, which is never met in TF-QKD lab experiments. The quantum channel for transmitting signal pulses is in an optical cable (96 fibers included). Part of the noise proceeds from the classical services running in some fibers in the optical cable. Fortunately, it can be filtered by a pair of cascaded DWDMs at the end of each quantum channel in Charlie to approximately 5.1×10^{-9}/pulse, which is acceptable for us, as shown in Fig. 2(a). The other part of the crosstalk noise is raised from the cw bright beam (same wavelength with the signal, generated from the master laser in Charlie) in the synchronization channel, which is also in the same optical cable. Thus it cannot be filtered, whether spectrally or temporally. We found that the crosstalk noise becomes more ignorable as the optical launch power of the cw bright beam decreases, which is shown in Fig. 2(b). To suppress the noise, we reduce the optical launch power of the master laser to about 5 dBm and increase the EDFA gain appropriately, resulting in a noise level of 3.6×10^{-9}/pulse. Still, a stable and high-efficiency injection can be ensured in this case.

Results.—In our field test, Alice and Bob send a total of 5.59×10^{12} pulse pairs, and obtain 2.79×10^{7} sifted key bits in the Z basis, including 27.84% error bits. According to the method shown in Ref. [37] and the data acquired in the experiment, there are at least 1.29×10^{7} untagged bits in the sifted keys, corresponding to an 11.07% phase flip error rate before AOPP. After AOPP, 5.84×10^{6} keys survive which contain 0.69% error bits. The number of untagged bits is 2.38×10^{6} with a corresponding phase flip error rate of 20.24%. With the finite-key effect being taken into consideration, we finally obtain a secure key rate of 4.80×10^{-8}/pulse, which is 170% higher than the absolute PLOB bound, 859% higher than the relative PLOB bound, and 2–4 orders of magnitude improvement than two comparable experiments over 400 km which were using a BB84 [42] and a measurement-device-independent QKD configuration [14], respectively. Figure 3 shows the performance of our work in terms of the simulation key rates, the achieved secure key rate, and the total efficiency of the polarization auto-alignment module and arrival time synchronization.

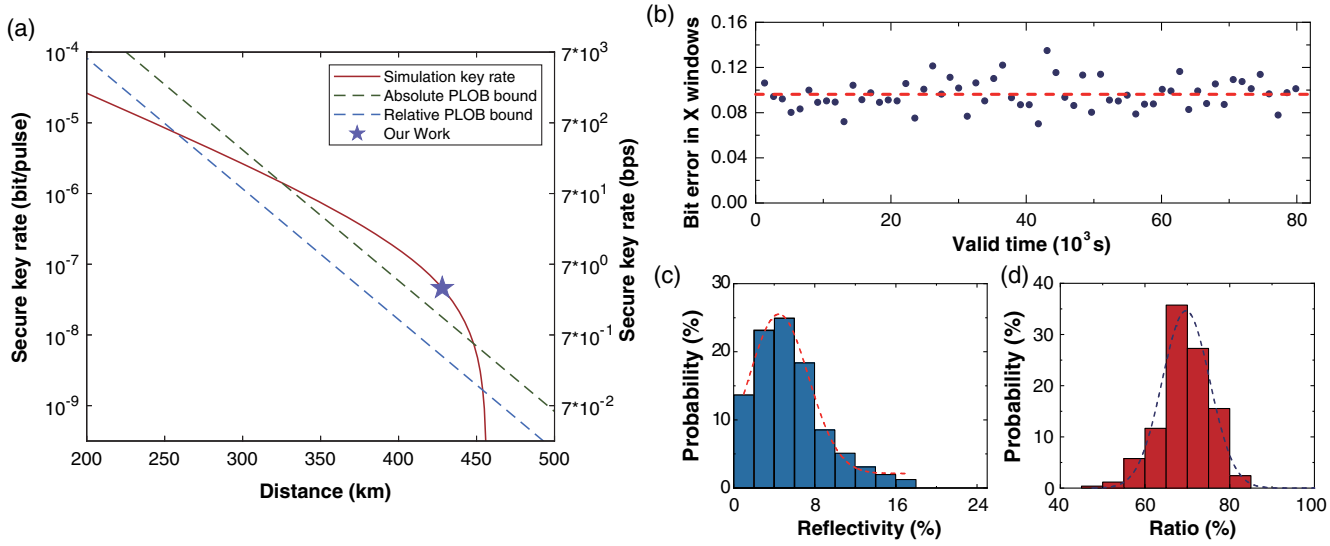

FIG. 3. (a) Experimentally and simulated secure key rates. The secure key rate (purple pentagram point) of our work is 4.80×10^{-8}/pulse, corresponding to 3.36 bps. The red curve is the simulation results using the parameters in Table I of Ref. [37]. The green and blue dashed line are the absolute PLOB bound (assuming the overall detection efficiency of Charlie $\eta_d = 1$) and the relative PLOB bound with $\eta_d = 28\%$, respectively. (b) The bit error rate in X windows. Each data point represents the effective clicks collected in 21.82 min on average. (c) The probability distribution of the reflectivity for the PBSs in Charlie, with real-time compensation in the overall experiment. The total efficiency of the polarization auto-alignment module is about 94% (the detail see Ref. [37]). (d) The probability distribution of the overlapping rate between the signal pulse and detection window in the overall experiment. The total overlapping is 70% (see details in Ref. [37]).

Conclusions.—Applying the SNS protocol [32], we have performed the first field test of TF-QKD over a 428 km deployed commercial fiber. It is the longest distance of terrestrial real-word QKD without relying on trusted relays, at present, and pushes the separation between two users beyond 300 km. The result demonstrated in our experiment exhibits the feasibility of the trusted-relayless QKD in practical circumstances between cities. It motivates future demonstration of an intercity-scale QKD network in the absence of the quantum repeater.

Compared to the 2.5 GHz system repetition rate of the existing BB84 protocol [42], our system's overall repetition rate is not high enough. However, the TF-QKD protocol has a higher requirement in time synchronization and calibration than the BB84 protocol, making it challenging to increase the TF-QKD system repetition significantly. Besides, the relative phase calculation and detection recovery decrease the effective repetition directly in our experiment. Fortunately, a novel wavelength-multiplexed approach for the relative phase calculation has been proposed and demonstrated [43]. It has the potential for a more advantageous effective repetition rate for quantum communication. Further extensions to higher key rates include utilizing the fiber link with lower attenuation and less crosstalk noise, and enhancing the laser and detector's performance.

This work was supported by the National Key R&D Program of China (2017YFA0303903, 2020YFA0309800), the Chinese Academy of Science, the National Fundamental Research Program, the National Natural Science Foundation of China (Grants No. 11875173, No. 61875182, and No. 11674193), China State Railway Group Co., Ltd. Scientific and Technological Research Project under Grant No. K2019G062, and Anhui Initiative in Quantum Information Technologies and Fundamental Research Funds for the Central Universities (WK2340000083).

Note added.—We note that related experimental work has been reported in Ref. [44]. Both our work and Ref. [44] are the field tests of SNS TF-QKD over almost the same deployed commercial fiber. However, we realize the wavelength synchronization with the assistance of the laser injection technique, which is off the shelf, mature, and easy to implement; while the wavelength synchronization system in Ref. [44] utilizes the time-frequency dissemination technology, which has less cross-talk noise and achieves a longer distance.

*xbwang@tsinghua.edu.cn
†tychen@ustc.edu.cn
‡pan@ustc.edu.cn

[1] C. H. Bennett and G. Brassard, in *Proceedings of the IEEE International Conference on Computers, Systems, and Signal Processing* (IEEE, New York, 1984), pp. 175–179.

[2] N. Gisin, G. Ribordy, W. Tittel, and H. Zbinden, Rev. Mod. Phys. **74**, 145 (2002).
[3] V. Scarani, H. Bechmann-Pasquinucci, N. J. Cerf, M. Dušek, N. Lütkenhaus, and M. Peev, Rev. Mod. Phys. **81**, 1301 (2009).
[4] S.-K. Liao, W.-Q. Cai, W.-Y. Liu, L. Zhang, Y. Li, J.-G. Ren, J. Yin, Q. Shen, Y. Cao, Z.-P. Li *et al.*, Nature (London) **549**, 43 (2017).
[5] F. Xu, X. Ma, Q. Zhang, H.-K. Lo, and J.-W. Pan, Rev. Mod. Phys. **92**, 025002 (2020).
[6] S. Pirandola, U. L. Andersen, L. Banchi, M. Berta, D. Bunandar, R. Colbeck, D. Englund, T. Gehring, C. Lupo, C. Ottaviani, J. L. Pereira, M. Razavi, J. S. Shaari, M. Tomamichel, V. C. Usenko, G. Vallone, P. Villoresi, and P. Wallden, Adv. Opt. Photonics **12**, 1012 (2020).
[7] C. Portmann and R. Renner, arXiv:2102.00021.
[8] W.-Y. Hwang, Phys. Rev. Lett. **91**, 057901 (2003).
[9] X.-B. Wang, Phys. Rev. Lett. **94**, 230503 (2005).
[10] H.-K. Lo, X. Ma, and K. Chen, Phys. Rev. Lett. **94**, 230504 (2005).
[11] S. L. Braunstein and S. Pirandola, Phys. Rev. Lett. **108**, 130502 (2012).
[12] H.-K. Lo, M. Curty, and B. Qi, Phys. Rev. Lett. **108**, 130503 (2012).
[13] Y.-H. Zhou, Z.-W. Yu, and X.-B. Wang, Phys. Rev. A **93**, 042324 (2016).
[14] H.-L. Yin, T.-Y. Chen, Z.-W. Yu, H. Liu, L.-X. You, Y.-H. Zhou, S.-J. Chen, Y. Mao, M.-Q. Huang, W.-J. Zhang, H. Chen, M. J. Li, D. Nolan, F. Zhou, X. Jiang, Z. Wang, Q. Zhang, X.-B. Wang, and J.-W. Pan, Phys. Rev. Lett. **117**, 190501 (2016).
[15] M. Lucamarini, Z. L. Yuan, J. F. Dynes, and A. J. Shields, Nature (London) **557**, 400 (2018).
[16] S. Pirandola, R. Laurenza, C. Ottaviani, and L. Banchi, Nat. Commun. **8**, 15043 (2017).
[17] M. Peev *et al.*, New J. Phys. **11**, 075001 (2009).
[18] D. Stucki, M. Legre, F. Buntschu, B. F. Clausen, N. Felber, N. Gisin, L. Henzen, P. Junod, G. Litzistorf, P. Monbaron *et al.*, New J. Phys. **13**, 123001 (2011).
[19] T.-Y. Chen, H. Liang, Y. Liu, W.-Q. Cai, L. Ju, W.-Y. Liu, J. Wang, H. Yin, K. Chen, Z.-B. Chen, C.-Z. Peng, and J.-W. Pan, Opt. Express **17**, 6540 (2009).
[20] J. F. Dynes, A. Wonfor, W. Tam, A. W. Sharpe, R. Takahashi, M. Lucamarini, A. Plews, Z. L. Yuan, A. R. Dixon, J. Cho *et al.*, npj Quantum Inf. **5**, 101 (2019).
[21] T.-Y. Chen, J. Wang, H. Liang, W.-Y. Liu, Y. Liu, X. Jiang, Y. Wang, X. Wan, W.-Q. Cai, L. Ju, L.-K. Chen, L.-J. Wang, Y. Gao, K. Chen, C.-Z. Peng, Z.-B. Chen, and J.-W. Pan, Opt. Express **18**, 27217 (2010).
[22] S. Wang, W. Chen, Z.-Q. Yin, Y. Zhang, T. Zhang, H.-W. Li, F.-X. Xu, Z. Zhou, Y. Yang, D.-J. Huang, L.-J. Zhang, F.-Y. Li, D. Liu, Y.-G. Wang, G.-C. Guo, and Z.-F. Han, Opt. Lett. **35**, 2454 (2010).
[23] Y.-L. Tang, H.-L. Yin, Q. Zhao, H. Liu, X.-X. Sun, M.-Q. Huang, W.-J. Zhang, S.-J. Chen, L. Zhang, L.-X. You, Z. Wang, Y. Liu, C.-Y. Lu, X. Jiang, X. Ma, Q. Zhang, T.-Y. Chen, and J.-W. Pan, Phys. Rev. X **6**, 011024 (2016).
[24] Y.-A. Chen *et al.*, Nature (London) **589**, 214 (2021).
[25] M. Sasaki *et al.*, Opt. Express **19**, 10387 (2011).
[26] M. Minder, M. Pittaluga, G. Roberts, M. Lucamarini, J. Dynes, Z. Yuan, and A. Shields, Nat. Photonics **13**, 334 (2019).
[27] Y. Liu, Z.-W. Yu, W. Zhang, J.-Y. Guan, J.-P. Chen, C. Zhang, X.-L. Hu, H. Li, C. Jiang, J. Lin, T.-Y. Chen, L. You, Z. Wang, X.-B. Wang, Q. Zhang, and J.-W. Pan, Phys. Rev. Lett. **123**, 100505 (2019).
[28] S. Wang, D.-Y. He, Z.-Q. Yin, F.-Y. Lu, C.-H. Cui, W. Chen, Z. Zhou, G.-C. Guo, and Z.-F. Han, Phys. Rev. X **9**, 021046 (2019).
[29] X. Zhong, J. Hu, M. Curty, L. Qian, and H.-K. Lo, Phys. Rev. Lett. **123**, 100506 (2019).
[30] X.-T. Fang, P. Zeng, H. Liu, M. Zou, W. Wu, Y.-L. Y.-J. Sheng, Y. Xiang, W. Zhang, H. Li *et al.*, Nat. Photonics **14**, 422 (2020).
[31] J.-P. Chen, C. Zhang, Y. Liu, C. Jiang, W. Zhang, X.-L. Hu, J.-Y. Guan, Z.-W. Yu, H. Xu, J. Lin, M.-J. Li, H. Chen, H. Li, L. You, Z. Wang, X.-B. Wang, Q. Zhang, and J.-W. Pan, Phys. Rev. Lett. **124**, 070501 (2020).
[32] X.-B. Wang, Z.-W. Yu, and X.-L. Hu, Phys. Rev. A **98**, 062323 (2018).
[33] C. Jiang, Z.-W. Yu, X.-L. Hu, and X.-B. Wang, Phys. Rev. Applied **12**, 024061 (2019).
[34] H. Xu, Z.-W. Yu, C. Jiang, X.-L. Hu, and X.-B. Wang, Phys. Rev. A **101**, 042330 (2020).
[35] X.-L. Hu, C. Jiang, Z.-W. Yu, and X.-B. Wang, Phys. Rev. A **100**, 062337 (2019).
[36] Z.-W. Yu, X.-L. Hu, C. Jiang, H. Xu, and X.-B. Wang, Sci. Rep. **9**, 3080 (2019).
[37] See Supplemental Material at http://link.aps.org/supplemental/10.1103/PhysRevLett.126.250502 for detailed theoretical scheme, detailed experimental technologies, and full experimental results, which includes Refs. [38–40].
[38] H. Chernoff, Ann. Math. Stat. **23**, 493 (1952).
[39] A. Vitanov, F. Dupuis, M. Tomamichel, and R. Renner, IEEE Trans. Inf. Theory **59**, 2603 (2013).
[40] C. Jiang, X.-L. Hu, H. Xu, Z.-W. Yu, and X.-B. Wang, New J. Phys. **22**, 053048 (2020).
[41] Z. L. Yuan, B. Fröhlich, M. Lucamarini, G. L. Roberts, J. F. Dynes, and A. J. Shields, Phys. Rev. X **6**, 031044 (2016).
[42] A. Boaron, G. Boso, D. Rusca, C. Vulliez, C. Autebert, M. Caloz, M. Perrenoud, G. Gras, F. Bussières, M.-J. Li, D. Nolan, A. Martin, and H. Zbinden, Phys. Rev. Lett. **121**, 190502 (2018).
[43] C. Clivati, A. Meda, S. Donadello, S. Virzì, M. Genovese, F. Levi, A. Mura, M. Pittaluga, Z. L. Yuan, A. J. Shields, M. Lucamarini, I. P. Degiovanni, and D. Calonico, arXiv:2012.15199.
[44] J.-P. Chen, C. Zhang, Y. Liu, C. Jiang, W.-J. Zhang, Z.-Y. Han, S.-Z. Ma, X.-L. Hu, Y.-H. Li, H. Liu, F. Zhou, H.-F. Jiang, T.-Y. Chen, H. Li, L.-X. You, Z. Wang, X.-B. Wang, Q. Zhang, and J.-W. Pan, arXiv:2102.00433.